Interferometric SAR observations of water level changes: Potential targets for future repeat-pass AIRSAR missions

Douglas E. Alsdorf
Department of Geography, University of California at Los Angeles, Los Angeles, CA 90095-1524, alsdorf@geog.ucla.edu, 310-794-4987.

Abstract:

Wetlands cover up to 6% of the earth's land surface and include hydrologic, biogeochemical flux and sediment transport processes that are key for understanding ecological and climatic changes. Measurements of water levels and changes are among the most fundamental observations that can be made throughout a wetland. Yet, surprisingly, almost no stage recording devices are located on any of the world's large, lowland floodplains. Instead, discharge is measured only in the main channels where flow is confined, unlike floodplains, where flow is not confined. The vast, inaccessible location of large wetlands such as the Amazon and Congo floodplains, require non-contact, remote methods of measuring floodplain water storage and related changes. My colleagues and I have recently discovered that interferometric processing of SAR data collected over inundated vegetation provides cm-scale changes in water levels across the Amazon floodplain. These results have been spatially integrated with a flow network, extracted from SAR imagery, to show that flow path distance is a controlling factor on water level changes, hence on storage.

Although interferometric SAR methods of measuring topographic changes related to earthquakes, volcanic activity, and glacial flows are well established, measuring water level changes is still under development. A number questions remain regarding the SAR and geomorphic parameters necessary for acquisitions of water level changes over flooded vegetation. Perhaps the most important question is "what are the relationships between radar frequency, interferometric coherence, and vegetation type that yield the most useful measurement of water level change?" Given that airborne platforms offer a greater scheduling flexibility than spaceborne platforms, AirSAR and others like it, present a great opportunity to explore the utility of expanding interferometric methods of measuring water level changes in flooded vegetation. Results would be extremely important for hydrologic and ecological investigations of wetland environments.

A. Introduction:

Wetlands cover five to eight million square kilometers globally [*Matthews and Fung,* 1986; *Matthews,* 1993; *Mitchell,* 1990], blanketing up to six percent of the earth's land surface. The flow of water through these floodplains is a control on both biogeochemical [e.g., carbon and methane, *Melack and Forsberg,* 2000] and sediment fluxes [e.g., *Dunne et al.,* 1998; *Smith and Alsdorf,* 1998]. Water storage in floodplains is also a key, governing parameter in continental-scale hydrologic models [*Coe,* 1998; *Vörösmarty et al.,* 1989; *Richey et al.,* 1989]. For example, *Coe* [1998; 2000] developed a water balance and transport model that simulates flow through rivers coupled with temporary storage in lakes and wetlands. Forcing the model with global

climate model (GCM) runoff estimates, *Coe* [2000] found that the addition of a wetlands component provided nearly 50% of the observed Nile River discharge in the Sudan. In another example, *Richey et al.* [1989] used Muskingum modeling and estimated the Amazon floodplain to mainstem exchange at 25% of the annual discharge at the mouth. These large percentages suggest that inaccurate knowledge of floodplain storage and subsequent discharge can lead to significant errors in hydrological, sediment flux, and biogeochemical models.

An understanding of the flooding dynamics and hydrologic exchange between rivers and related floodplains relies on measurements of water levels recorded at gauging stations along a main channel and within a floodplain. For many remote basins, however, the lack of floodplain stage recording devices results in poorly constrained estimates of floodplain water storage. For example, only one of the ~8000 lakes on the Amazon floodplain has been monitored for more than a brief period [*Lesack and Melack,* 1995]. Instead, modeling efforts have begun to rely on remotely sensed observations that either directly record water surface elevation using satellite borne radar altimetry [e.g., *Birkett,* 1998; *Koblinsky et al.,* 1993] or infer stage and discharge from relationships between main channel gauge data and remotely sensed inundated area [e.g., *Sippel et al.,* 1998; *Smith,* 1997; *Smith et al.,* 1995, 1996; *Vörösmarty et al.,* 1996].

Given the vast size and remote location of many large basins such as the Amazon and Congo, airborne and satellite observations remain the only viable approach to constraining and validating basin scale hydrologic models. However, the altimetric and inundation area approaches for measuring floodplain storage are limited. Conventional radar altimetry is a profiling tool with a satellite track spacing of ~300 km, thus it can miss significant portions of a floodplain. Inferring floodplain storage and discharge from inundated area requires calibration with ground discharge data and does not work well in environments where small changes in water heights yield little change in surface area yet significant changes in flow. These approaches typically regress area, derived from temporal maps of inundation, with discharge, derived from in-channel gauge data, to predict floodplain discharge. However, mathematically, this method actually results in a prediction of the combined discharges from main channels and adjacent floodplains.

My colleagues and I have recently demonstrated that interferometric processing and analyses of synthetic aperture radar (SAR) data can yield centimeter-scale measurements of water level changes throughout inundated floodplain vegetation [*Alsdorf et al.,* 2000; 2001a; 2001b]. Furthermore, we have shown that these local observations across individual floodplain water bodies can be spatially integrated in a geographic information system (GIS) to yield estimates of floodplain storage change [*Alsdorf et al.,* 2001c; *Alsdorf,* 2001d]. A key aspect of our interferometric method is that it produces a *volumetric* measure of water storage change that is independent of ground-based observations.

Given (1) that changes in floodplain storage for many of the world's large, lowland river systems are estimated to be a significant portion of total basin discharge (e.g., 25% to 50% is typical), (2) that biogeochemical and sediment transport studies rely on accurate floodplain storage, (3) that flooding hazard studies require measures of storage and transport capacity, and (4) that in-situ

gauging of vast, remote floodplains is cost prohibitive, a remotely-sensed system of understanding floodplain water storage and subsequent exchange with main-channel rivers is required to improve models of continental-scale hydrology and their coupling with GCMs.

B. How Interferometric SAR Measures Water Level Changes:

Interferometric processing of SAR data has already been used to map the centimeter-scale changes in topography related to earthquakes, volcanic activity, and groundwater flux [e.g., *Massonnet et al.*, 1993; *Zebker et al.*, 1994; *Wicks et al.*, 1998; *Hoffman et al.*, 2001], to map the velocity field of flowing glaciers [e.g., *Goldstein et al.*, 1993], and to map the atmospheric water vapor changes resulting from storms [e.g., *Hanssen et al.*, 1999]. The processing method requires two SAR image acquisitions from identical (or nearly identical) viewing geometries before and after the displacement phenomenon; co-registration of the two images to a sub-pixel accuracy; and subtraction of the complex phase and amplitude values at each SAR image pixel. The value of the resulting interferometric phase at each pixel varies between -pi and +pi and is primarily a function of the distance between the radar antenna positions during acquisition (i.e., the platform baseline), topographic relief, surface displacement, and the degree of correlation between the individual scattering elements that comprise each pixel location (i.e., coherence, *Rosen et al.*, 1996).

Because imaging SAR techniques use an antenna that transmits the radar pulse at an off-nadir look-angle, the high dielectric contrast between smooth open-water and air causes most of the pulse energy to be reflected away from the antenna (i.e., specular reflections). Furthermore, depending on radar wavelength, the water surface can appear in a continuous state of change (i.e., roughened), resulting in complete loss of temporal coherence between SAR images acquired at different times. Thus, previous investigators assumed that interferometric analyses of SAR data would *not* reveal changes in water levels. However, radar pulse interactions with inundated vegetation typically follow a double-bounce path that includes the water surface and trunks of vegetation, which returns most of the energy to the antenna [*Hess et al.*, 1995]. This returned energy enables interferometric phase measurements of the earth, vegetation trunks, and water surfaces encountered along the pulse travel-path. We have used L-HH-band SAR data from the Space Shuttle Imaging Radar mission (SIR-C mission, *Alsdorf et al.*, 2000; 2001a; Figure 1) and from the Japanese Earth Resources Satellite (JERS-1, *Alsdorf et al.*, 2001b; Figure 2) to demonstrate that centimeter-scale changes in water levels beneath flooded vegetation *can* be measured interferometrically, despite 24-hour and 44-day temporal baselines, respectively.

However, the method has not been attempted with non-HH polarizations such as HV or VV (horizontally and vertically transmitted and received polarizations) nor with non-L-band wavelengths (L-band = 24 cm). Furthermore, the vegetation characteristics required to produce the double-bounce travel path have not been explored. Our initial work suggests that both dense forest canopies and sparsely distributed, dead, leafless trees will produce a returned pulse.

C. Scaling Local Observations of Water Level Change to Floodplain Storage:

For all floodplains, the main channel is the major discharge outlet. We have interferometrically measured water level changes across individual floodplain water bodies on the central Amazon floodplain. These changes were recorded over a 24-hour period during mainstem recessional

flow in mid-October and are represented as d*h*/d*t* where *h* is the water surface elevation and *t* is time. These local observations of d*h*/d*t* distributed across the floodplain must be spatially linked to the main channel to determine floodplain storage changes. The advent of the digital elevation model (DEM) from the February 2000 Shuttle Radar Topography Mission (SRTM) will greatly facilitate the identification of flow paths that connect each floodplain observation of d*h*/d*t* to the main channel. In the interim, we have recently determined that major floodplain flow paths can be identified in SAR amplitude imagery using stream network extraction algorithms [*Alsdorf,* 2001d]. In general, low SAR amplitudes are recorded over open water where elevations are also expected to be the lowest whereas high backscatter values are typically found over non-inundated, higher elevation terrain [*Hess et al.,* 1995; 2001].

Floodplain storage changes are found by spatially integrating the local interferometric observations of d*h*/d*t* across a floodplain [*Alsdorf et al.,* 2001c]. The extracted flow path network guides the pattern of linkage between floodplain locations and the main channel. Because non-flooded areas cannot have an associated d*h*/d*t*, the volume encapsulated by the extrapolation is multiplied by the percentage of inundated floodplain to produce the final estimate of floodplain storage change. During mid-recessional flow across the central Amazon floodplain, this process yields a storage change estimate of 4600 m^3/s (+400 m^3/s and –900 m^3/s) for the extracted network between Itapeua and Manacapuru [*Alsdorf,* 2001d].

Water levels and changes across floodplains have not been explicitly measured inputs in previous continental-scale hydrologic models. Instead, floodplain storage values are calculated by *assuming* that floodplain water levels and temporal fluctuations are equivalent to those of the main river channel. The interferometric observations like those of Figure 1 suggest that this assumption may not be justified. The difference between assumed floodplain storage change values and the interferometric estimate is 30%, with model-based change estimates of 6500 m^3/s [*Richey et al.,* 1989]. However, the model-based estimates are built on 15 years of annual, main-channel gauge averages whereas the interferometric estimate is built from a 24-hour snapshot across the floodplain.

D. Remaining Questions and Airborne SAR Platforms:

Our previous work has focused on the Amazon floodplain and resulted in the intriguing difference in floodplain storage change estimates between our interferometric procedure and a continental-scale hydrologic model. The interferometric result was collected in October 1994, during mid-recessional flow on a 300 km long reach of the Amazon floodplain and, thus, may be temporally and spatially unique. However, if this difference is generally true, being applicable to the entire Amazon River during both recession and inundation, and if similar results were found over other large, continental-scale floodplains, then continental-scale hydrologic models and their coupling to GCMs require reanalysis. The variety of radar polarizations and frequencies available on AirSAR present a unique opportunity to test the generality of our interferometric method. The following questions present opportunities that could be addressed with AirSAR.

D.1 Can Large Perpendicular Baselines at L-Band Yield Water Level Changes?

The observed interferometric phase measures both the local topography and also any surface

displacements that occur between SAR acquisitions. To separate these components, either a synthetic interferogram based on a DEM ("two-pass method", *Massonnet et al.,* 1993) or additional SAR interferograms free of displacement phenomenon ("multi-pass method", *Zebker et al.,* 1994), can be subtracted from the observed phase. Because water surface elevations are constantly changing during the temporal baseline of typical satellite acquisitions, the topographic phase cannot be easily extracted using additional satellite SAR images, which suggests that the two-pass method will likely be required for satellite based approaches. The TopSAR mode of AirSAR allows immediate acquisition of topography without intervening temporal changes in water levels, thus an AirSAR mission could acquire both the necessary DEM and additional repeat passes.

The amount of topographic relief captured by one interferometric phase cycle, from –pi to +pi, is a function of the perpendicular component of the baseline. Short perpendicular components yield more topographic relief per phase cycle than long baselines, thus a more reliable estimate of surface change. Our previous two demonstrations of the interferometric method for measuring d*h*/d*t* used L-HH data with perpendicular baselines between satellite acquisitions of +63 m (SIR-C) and –118 m (JERS-1). These short baselines indicate that 0.5 radians of phase are equivalent to 15-20 m of topographic relief, whereas depending on look angle, the same 0.5 radians are also equivalent to about 1 cm of water surface change.

On the Amazon floodplain, the local topographic relief surrounding phase observations is typically less than 20 m. Thus, measurements of d*h*/d*t* on floodplains that presently lack DEM data, such as the Amazon, require small perpendicular baselines and water level changes in excess of 1 cm (i.e., the topographic phase component can be ignored). However, the use of TopSAR DEMs should alleviate this restriction, allowing much larger baselines. Note that the critical baseline for L-band, where coherence breaks down because of look angle restrictions, is about 4 km at satellite altitudes [*Zebker and Villasenor,* 1992].

D.2 Is L-Band Coherence a Function of Temporal Baseline?

Over land surfaces, where changes in soil moisture, vegetation, and freeze/thaw cycling cause random changes in the structure and dielectric properties of the scattering elements, interferometric coherence typically diminishes with increasing time between SAR acquisitions. Over inundated vegetation, the scattering elements consist of the water surface and vegetation trunks. For short time periods, say 24-hours, the water surface is likely to experience a greater change in structure than the trunks of vegetation (i.e., wave action on the water surface). Thus, short-term temporal coherence is probably a function of the stability of the water surface (i.e., dielectric changes in the air-water interface are assumed to be minor). Across seasonal growth periods, however, vegetation changes will also affect coherence. During the 24-hours separating SIR-C acquisitions, coherence was maintained (Figure 1), thus we initially assumed that the heavy Amazon forest canopy prevented wind roughening of the water surface during the one-day period. Yet given the low vegetation density and large water surface of the lake in Figure 2, it is doubtful that wind and wave action would be similarly subdued for the 44-day temporal baseline of the JERS-1 interferogram. Nevertheless, strong coherence is maintained across the entire JERS-1 image.

To separate the affects on coherence from a changing water surface and from vegetation,

comparisons between inundated areas where one of the parameters is held constant are necessary. Locations where the vegetation over the water surface is dead, still provide a radar double-bounce travel-path but do not confound coherence with vegetation changes. Conversely, locations where the water is stagnant, but the vegetation experiences seasonal changes, reduce the water surface affects on coherence. If L-band coherence does not vary with time, then subtle variations in d*h*/d*t* over wetlands with flooded vegetation can be measured with interferometric SAR techniques. For example, annual water level changes throughout the Florida Everglades are less than ~2 m and are typically about 1 m with month-to-month variations between 10 and 20 cm [*SFWMD*, 2001]. Interferograms with long temporal baselines would be effective for measuring seasonal variations in d*h*/d*t*, and subsequently yield images of floodplain storage change.

D.3 Does L-Band Coherence Vary With Vegetation Type and Density?

The Amazon floodplain and Florida Everglades, like most tropical wetlands, contain a rich variety of vegetation. For example, *Hess et al.* [2001] have used SAR amplitude images to map seasonal variations in Amazon floodplain habitats marked by herbaceous vegetation, shrubs, forests, woodlands, and aquatic macrophytes. Contrasting this variety are the dead, leafless trees within the lake of Figure 2. We have an extensive archive of high-resolution airborne videography throughout the Amazon floodplain available for determinations of vegetation density to couple with the classification schemes. Similarly, high-resolution airborne videography onboard AirSAR would provide necessary imagery for determinations of vegetation type and density. This imagery could be classified and compared to repeat-pass AirSAR interferometric products to determine coherence variations.

D.4. What is the Variation in Coherence Between Differing Polarizations and Wavelengths?

Our initial results from the SIR-C interferometric data suggest that coherence is strongest over flooded vegetation for L-HH compared to L-HV and C-HH [*Alsdorf et al.*, 2001a]. However, these results were derived over a 24-hour period during recessional-flow and related habitat seasonal growth cycle. Furthermore, the vegetation types and densities were not delineated in this basic assessment. Although C-band radar pulses backscatter from the dense forest canopy, rather than the underlying ground or water surface, double-bounce travel paths are known for C-band data over inundated macrophytes and small shrubs [*Hess et al.*, 1995]. Given the sparse, dead vegetation over the lake of Figure 2, its probable that C-band data would follow a double-bounce travel path in similar environments.

Conclusions:

A number of interferometric SAR missions on both satellite and airborne platforms have been proposed to NASA over the past four years. The missions have been focused on improving knowledge of earthquake, volcanic, and glacier processes through interferometric mapping of related topographic displacements. These methodologies are well-established with several hundred publications. The unknown parameters outlined in hypotheses D.1 through D.4, suggest that measuring floodplain storage change with interferometric SAR methods is still in an early stage of development. Ideally, future missions would include floodplain storage change as a potential target, especially given the global distribution and vast areas encompassed by wetlands

as well as the climatic impacts of wetland biogeochemistry and hydrology. Questions D.1 through D.4 help define the core parameters necessary for identifying SAR antenna and mission design. Results of these questions could be compared to proposed SAR missions to determine the applicability of interferometrically measuring d*h*/d*t* within the mission criteria. Ideally, future missions focused on geodynamic and glaciologic processes can be similarly focused on floodplain storage change without loss to core mission requirements.

G. References Cited:

Alsdorf, D.E., J. M. Melack, T. Dunne, L.A.K. Mertes, L.L. Hess, and L.C. Smith. 2000. Interferometric radar measurements of water level changes on the Amazon floodplain. *Nature* (404): 174-177.

Alsdorf, D.E., L.C. Smith, and J.M. Melack. 2001a. Amazon floodplain water level changes measured with interferometric SIR-C radar. *IEEE Transactions in Geoscience and Remote Sensing* (39): 423-431.

Alsdorf, D., C. Birkett, T. Dunne, J. Melack, and L. Hess. 2001b. Water level changes in a large Amazon lake measured with spaceborne radar interferometry and altimetry. *Geophysical Research Letters* (28): 2671-2674.

Alsdorf, D.E., T. Dunne, L.A.K. Mertes, J. M. Melack, L.L. Hess, and L.C. Smith. 2001c. Water storage and discharge across the central Amazon floodplain measured with spaceborne interferometric radar, w*ill be accepted after minor revisions, Water Resources Research*.

Alsdorf, D.E., 2001d. Water storage of the central Amazon floodplain measured with GIS and remote sensing imagery. *in review with Annals of the Association of American Geographers*.

Bates, P.D., M.D. Stewart, A. Desiter, M.G. Anderson, J.-P. Renaud, and J.A. Smith, Numerical simulation of floodplain hydrology, *Water Resources Research, 36,* 2517-2529, 2000a.

Birkett, C.M. 1998. Contribution of the TOPEX NASA radar altimeter to the global monitoring of large rivers and wetlands. *Water Resources Research* (34): 1223-1239.

Coe, M.T. 1998. A linked global model of terrestrial hydrologic processes: Simulation of modern rivers, lakes, and wetlands. *Journal of Geophysical Research* (103): 8885-8899.

Coe, M.T. 2000. Modeling terrestrial hydrological systems at the continental scale: Testing the accuracy of an atmospheric GCM. *Journal of Climate* (13): 686-704.

Dunne, T., L.A.K. Mertes, R.H. Meade, J.E. Richey, and B.R. Forsberg. 1998. Exchanges of sediment between the flood plain and channel of the Amazon River in Brazil. *GSA Bulletin* (110): 450-467.

Goldstein, R.M., H. Engelhardt, B. Kamb, and R.M. Frolich, "Satellite radar interferometry for monitoring ice sheet motion: Application to an Antarctic ice stream," *Science* vol. 262, pp. 1525-1530, 1993.

Goldstein, R.M., H.A. Zebker, and C.L. Werner, Satellite radar interferometry: Two-dimensional phase unwrapping, *Radio Science*, vol. 23, pp. 713-720, 1988.

Hanssen, R.F., T.M. Weckwerth, H.A. Zebker, and R. Klees, High-resolution water vapor mapping from inteferometric radar measurements, *Science,* v. 283, p. 1297-1299, 1999.

Hess, L.L., J.M. Melack, S. Filoso, and Y. Wang, Delineation of inundated area and vegetation along the Amazon floodplain with SIR-C synthetic aperture radar, *IEEE Trans. Geosci. Remote Sensing,* vol. 33, pp. 896-904, 1995.

Hess, L.L., J.M. Melack, and L.A.K. Mertes, 2001, Mapping Floodplain Habitats of the Amazon River Using Multi-temporal SAR and River Stage Data. *in review with* R*emote Sensing of the Environment.*

Hoffmann, J., H.A. Zebker, D.L. Galloway, and F. Amelung, Seasonal subsidence and rebound in Las Vegas Valley, Nevada, observed by synthetic aperture radar interferometry, *Water Resources Research,* Vol. 37, pgs. 1551-1566, 2001.

Koblinsky, C.J., R.T. Clarke, A.C. Brenner, and H. Frey. 1993. Measurement of river level variations with satellite altimetry. *Water Resources Research* (6): 1839–1848.

Lesack, L.F.W. and J.M. Melack. 1995. Flooding hydrology and mixture dynamics of lake water derived from multiple sources in an Amazon floodplain lake. *Water Resources Research* (31): 329-345.

Massonnet, D., M. Rossi, C. Carmona, F. Adragna, G. Peltzer, K. Feigl, and T. Rabaute, The displacement field of the Landers earthquake mapped by radar interferometry, *Nature*, vol. 364, pp. 138-142, 1993.

Matthews, E. and I. Fung, Methane emission from natural wetlands: Global distribution, area, and environmental characteristics of sources, *Global Biogeochemical Cycles*, vol. 1, pp. 61-86, 1987.

Matthews, E., "Wetlands", in Atmospheric Methane: Sources, Sinks, and Role in Global Change, edited by M.A.K. Khalil, pp. 314-361, Springer-Verlag, Berlin, 1993.

Melack, J.M. and B.R. Forsberg. 2000. Biogeochemistry of Amazon floodplain lakes and associated wetlands, in *The Biogeochemistry of the Amazon Basin and its Role in a Changing World*, M.E. McClain, R.L. Victoria, and J.E. Richey Eds. Oxford Univ. Press, New York, in press.

Mertes, L.A.K., Rates of flood-plain sedimentation on the central Amazon River, *Geology, 22*, 171-174, 1994.

Mertes, L.A.K., D.L. Daniel, J.M. Melack, B. Nelson, L.A. Martinelli, and B.R. Forsberg. 1995. Spatial patterns of hydrology, geomorphology, and vegetation on the floodplain of the Amazon River in Brazil from a remote sensing perspective. *Geomorphology* (13): 215-232.

Mertes, L.A.K., T. Dunne, and L.A. Martinelli. 1996. Channel-floodplain geomorphology along the Solimões-Amazon River, Brazil. *GSA Bulletin* (108): 1089-1107.

Mertes, L.A.K. 1997. Documentation and significance of the perirheic zone on inundated floodplains. *Water Resources Research* (33): 1749-1762.

Mitchell, G.J., Foreward to wetland creation and restoration. In: *Wetland Creation and Restoration: The Status of the Science*, Kusler, J. and Kentula, M. (eds.), Island Press, Washington D.C., p. ix-x.

Nicholas, A.P., and D.E. Walling, Numerical simulation of floodplain hydraulics and suspended sediment transport and deposition, *Hydrological Processes, 12*, 1339-1355, 1998.

Richey, J.E., L.A.K. Mertes, T. Dunne, R.L. Victoria, B.R. Forsberg, A.C.N.S. Tancredi, and E. Oliveira. 1989. Sources and routing of the Amazon River flood wave. *Global Biogeochemical Cycles* (3): 191-204.

Rosen, P.A., Hensley, S., Zebker, H.A., Webb, F.H. and Fielding, E.J. Surface deformation and coherence measurements of Kilauea Volcano, Hawaii, from SIR-C radar interferometry. *J. Geophysical Res.* 101, 23109-23125, 1996.

Sippel, S.J., S.K. Hamilton, J.M. Melack, and E.M.M. Novo. 1998. Passive microwave observations of inundation area and the area/stage relation in the Amazon River floodplain. *International Journal of Remote Sensing* (19): 3055-3074.

Smith, L.C., Isacks, B.L., Bloom, A.L., and A.B. Murray, Estimation of discharge from three braided rivers using synthetic aperture radar (SAR) satellite imagery: Potential application to ungaged basins, *Water Resources Research, 32*(7), 2021-2034, 1996.

Smith, L.C., Isacks, B.L., Forster, R.R., Bloom, A.L., and I. Preuss, Estimation of discharge from braided glacial rivers using ERS-1 SAR: First results, *Water Resources Research, 31*(5), 1325-1329, 1995.

Smith, L.C. 1997. Satellite remote sensing of river inundation area, stage, and discharge: A review. *Hydrological Processes* (11): 1427-1439.

Smith, L.C. and D.E. Alsdorf, Control on sediment and organic carbon delivery to the Arctic Ocean revealed with space-borne synthetic aperture radar: Ob' River, Siberia, *Geology*, v. 26, n. 5, pp. 395-398, 1998.

SFWMD, 2001, South Florida Water Management District, Hydrologic Systems Modeling Group, http://glacier.sfwmd.gov/org/pld/hsm/models/

Vörösmarty, C.J., B. Moore III, A.L. Grace, and M.P. Gildea. 1989. Continental scale models of water balance and fluvial transport: An application to South America. *Global Biogeochemical Cycles* (3): 241-265.

Vörösmarty, C.J., C.J. Willmott, B.J. Choudhury, A.L. Schloss, T.K. Stearns, S.M. Robeson, and T.J. Dorman. 1996. Analyzing the discharge regime of a large tropical river through remote sensing, ground-based climatic data, and modeling. *Water Resources Research* (32): 3137-3150.

Wicks, C., W. Thatcher, and D. Dzurisin, Migration of fluids beneath Yellowstone caldera inferred from satellite radar interferometry, *Science*, v. 282, p. 458-462, 1998.

Zebker, H.A., P.A., Rosen, R.M. Goldstein, A. Gabriel, and C.L. Werner, On the derivation of coseismic displacement fields using differential radar interferometry: The Landers earthquake, *J. Geophysical Res.*, vol. 99, pp. 19617-19634, 1994.

Zebker, H.A. and J. Villasenor, Decorrelation in interferometric radar echoes, *IEEE Transactions on Geoscience and Remote Sensing* v. 30, p. 950-959, 1992.

.
.
.
.
.
.

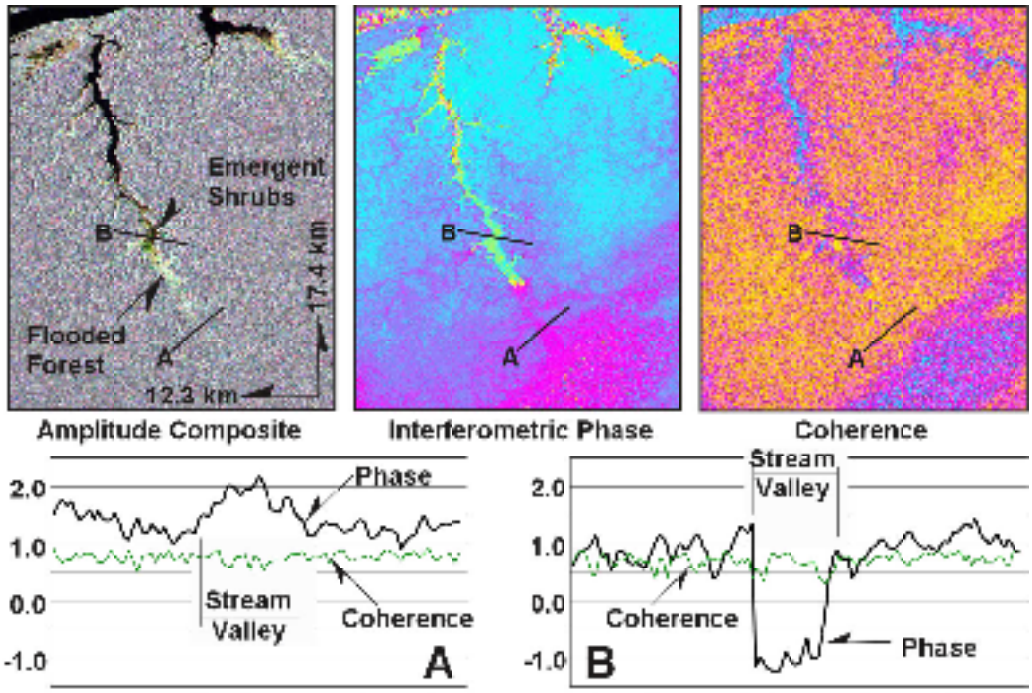

Figure 1. Amplitude composite (where SIR-C C-band HH-polarization intensities are colored red, L-IIII are green, and L-IIV are blue, left), flattened wrapped interferogram, and coherence images for a tributary of the Purus River near the confluence with the Amazon. Profiles of phase and coherence values extracted from the images show the valley topography in (A) and one-day stage decrease across inundated vegetation in (B). Atmospheric distortions run diagonally across the lower-right in the phase and coherence images. After *Alsdorf et al.*, 2001a.

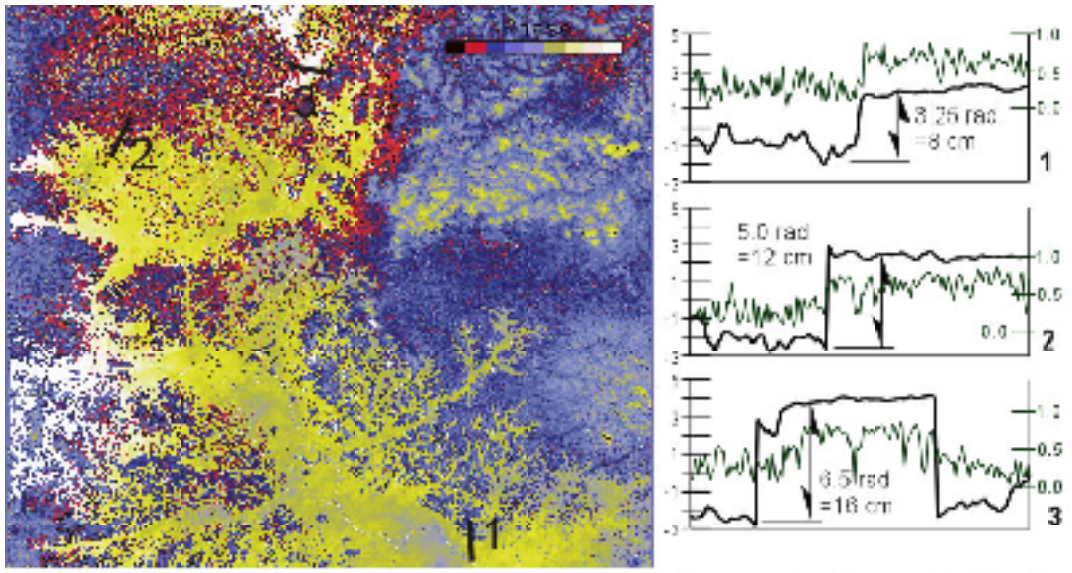

Figure 2. JERS-1 flattened and unwrapped interferometric phase calculated from data collected on February 14 and March 30, 1997. Image is about 70 x 70 km. Profiles of phase (bold black line, associated with radian values on left ordinate) and coherence (thin green line, associated with right ordinate) are plotted on right side of figure. After *Alsdorf et al.*, 2001b.